

Locating the missing superconducting electrons in overdoped cuprates

Fahad Mahmood,¹ Xi He,^{2,3} Ivan Božović,^{2,3} and N. P. Armitage¹

¹*The Institute for Quantum Matter, Department of Physics and Astronomy,
The Johns Hopkins University, Baltimore, MD 21218 USA.*

²*Brookhaven National Laboratory, Upton, NY 11973, USA.*

³*Applied Physics Department, Yale University, New Haven, Connecticut 06520, USA.*

(Dated: February 26, 2018)

Overdoped high-temperature cuprate superconductors have been widely believed to be described by the physics of d -wave BCS-like superconductivity. However, recent measurements [1] indicate that as the doping is increased, the superfluid density decreases smoothly to zero rather than increasing as expected by BCS theory in the absence of disorder. Here, we combine time-domain THz spectroscopy with kHz range mutual inductance measurements on the *same* overdoped $\text{La}_{2-x}\text{Sr}_x\text{CuO}_4$ films to determine both the superfluid and the uncondensed carrier density as a function of doping. A significant fraction of the carriers remains uncondensed in a wide Drude-like peak even as $T \rightarrow 0$, which, when taken with the linear-in-temperature superfluid density, is inconsistent with existing theories for the role of disorder in suppressing the superfluid density in a d -wave superconductor. Our almost eight orders of magnitude in measurement frequency range gives us a unique look at the low frequency spectral weight distribution, which may suggest the presence of quantum phase fluctuations as the critical doping is approached.

Underdoped cuprate superconductors exhibit various forms of structural, magnetic and electronic phases whose relationships with superconductivity are not fully understood [2]. However, overdoped cuprates have been believed to be simpler and well-described in terms of conventional BCS-like physics because of the high carrier density on the overdoped side [3]. This interpretation has been supported by the observation of a large and well defined Fermi surface in both photoemission [4] and quantum oscillation [5] experiments. However, other studies on overdoped cuprates indicate anomalies and for instance it has been found that the superfluid density was lower than expected [6–10]. If the physics of overdoped cuprates is indeed BCS-like, then in the absence of disorder the zero-temperature superfluid density n_{s0} should be set by the total carrier density.

Recent work by Božović et.al. [1], using kHz range mutual inductance (MI) measurements on thousands of overdoped $\text{La}_{2-x}\text{Sr}_x\text{CuO}_4$ films provides strong evidence that n_{s0} is indeed much lower than expected and decreases smoothly to zero as $T_c \rightarrow 0$, despite the fact that the superfluid density of the films shows a linear temperature dependence down to the lowest measured temperatures. This naturally leads to two important

questions: (1) Where are the “missing” carriers that do not condense into the superfluid condensate? And (2) why do they not condense? These issues are at the heart of the superconductivity debate in cuprates.

To answer these questions, we utilize time-domain THz spectroscopy (TDTS) in conjunction with kHz range MI measurements (almost eight orders of magnitude in measurement frequency range) to systematically track both the condensate and the free carrier spectral weight as a function of doping for overdoped $\text{La}_{2-x}\text{Sr}_x\text{CuO}_4$ films. We find that a significant fraction of the total spectral weight remains uncondensed as $T \rightarrow 0$ and manifests as a Drude-like peak at frequencies comparable to the theoretical weak coupling BCS gap. Taken with the linearity of the superfluid density with temperature, our observations cannot be reconciled with extant theories of a BCS-type d -wave superconductor in the presence of impurity scattering. Analysis of the frequency dependence of the spectral weight distribution points to the presence of significant quantum phase fluctuations. This limits any mean-field description of the superconducting transition on the overdoped side of the cuprate phase diagram.

Dynamical measurements such as TDTS are sensitive probes of the superconducting response at the relevant energy scales and allow us to independently determine both the real and imaginary parts of the frequency dependent conductivity $\sigma(\nu)$ [11]. Figure 1 shows the real $\sigma_1(\nu)$ and imaginary $\sigma_2(\nu)$ conductivities at different temperatures for an overdoped LSCO film ($x = 0.23$) with $T_c = 27.5$ K. At temperatures much greater than T_c , $\sigma_1(\nu)$ is frequency independent while $\sigma_2(\nu)$ is small, which is consistent with the behavior of a normal metal at frequencies well below the scattering rate. As the temperature is lowered across T_c , $\sigma_1(\nu)$ first rises and then decreases as spectral weight at higher frequencies is transferred to frequencies below the measurement range in the superconducting state. Similarly, below T_c , $\sigma_2(\nu)$ develops a $1/\nu$ -like dependence as the low frequency spectral weight condenses into a delta function at $\nu = 0$. However, even down to the lowest temperatures in the superconducting state ($T = 1.6$ K), $\sigma_1(\nu)$ remains comparable in size to the normal-state $\sigma_1(\nu)$ (Fig. 1c). A similar residual $\sigma_1(\nu)$ as $T \rightarrow 0$ has also previously been observed in cuprate $\text{Bi}_2\text{Sr}_2\text{CaCu}_2\text{O}_{8+\delta}$ films for a range of dopings [12, 13]. Such observations are incompatible with conventional BCS-like behavior in the absence of impurity scattering where nearly all the low frequency spectral weight should condense into a $\nu = 0$ delta func-

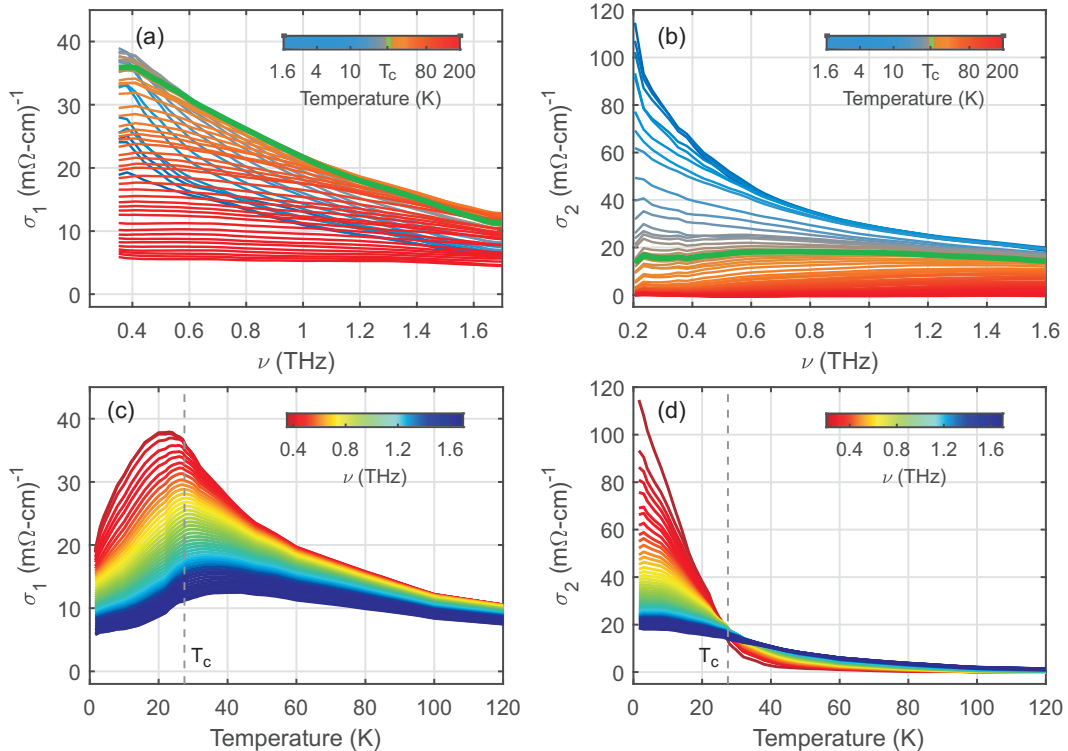


FIG. 1: **THz optical conductivity of an $x = 0.23$ $\text{La}_{2-x}\text{Sr}_x\text{CuO}_4$ thin film ($T_c = 27.5$ K).** Real (a) and imaginary (b) parts of the conductivity as a function of frequency at different temperatures. Green curve indicates the conductivity at T_c . Real (c) and imaginary (d) parts of the conductivity as a function of temperature at different frequencies. Vertical dashed lines denote T_c .

tion and consequently $\sigma_1(\nu)$ at THz frequencies should be negligible in the $T \rightarrow 0$ limit.

To study this further, we directly compare the measured $\sigma_1(\nu)$ in the normal state and in the limit $T \rightarrow 0$ for a range of overdoped LSCO films. Figures 2a, 2b and 2c show $\sigma_1(\nu)$ at temperatures above and below T_c for the superconducting films with $T_c = 27.5$ K, 13.5 K and 7 K respectively. The carrier spectral weight (S) contributing to the finite frequency conductivity is directly proportional to the area under the $\sigma_1(\nu)$ curve i.e. $\int_{0+}^{\infty} \sigma_1(\nu) d\nu = \frac{\pi}{2} S$. Based on this, it is apparent from Fig. 2a-c that a significant fraction of the normal state spectral weight (S_n) remains uncondensed at THz frequencies in the limit $T \rightarrow 0$. Moreover, the ratio of the uncondensed spectral weight (S_u) to the normal spectral weight becomes even greater (i.e. more anomalous) for the more overdoped films. This behavior can be quantified by fitting $\sigma_1(\nu)$ at each doping and temperature to a single Drude peak i.e. $\sigma_1(\nu) = S\tau/(1 + \nu^2\tau^2)$ (dashed lines on Fig. 2a-c). Figure 2e shows that the ratio of the uncondensed spectral weight to the normal state spectral weight monotonously approaches unity as the critical doping is approached on the overdoped side i.e. $S_u/S_n \rightarrow 1$ as $T_c \rightarrow 0$.

This observation naturally answers the first question raised above i.e. where is the “missing” spectral weight? Bozovic et. al. [1] observed a singular decrease in the superfluid density as $T_c \rightarrow 0$ suggesting that a large fraction of the carriers did not condense. Our results

indicate that these “missing” carriers remain in a THz wide Drude-like peak down to $T = 0$. To corroborate whether these are indeed the “missing” carriers, we have performed two-coil mutual inductance (MI) measurements on the *same* films to extract the spectral weight in the superconducting delta function (S_δ). Figure 2d shows S_δ as a function of temperature as obtained from the penetration depth (λ) from MI data ($S_\delta = \frac{1}{2\pi\mu_0\lambda^2}$) for the $x = 0.23$ (see Methods for details). As expected from previous MI measurements on overdoped LSCO films [1], $S_\delta(T)$ is essentially linear with T down to the lowest temperature. Similar results are obtained for the other dopings. We extrapolate the data to obtain S_δ at $T = 1.6$ K to directly compare with S_n and S_u obtained from TDTS at the same temperature for a range of dopings (Fig. 2e). In the context of the Ferrel-Glover-Tinkham (FGT) sum rule, $S_n = S_\delta + S_u$. Consequently, if our measured S_u is indeed due to the “missing” carriers, then $[S_\delta + S_u]/S_n = 1$ regardless of doping. As shown in Fig. 2e $S_\delta/S_n \rightarrow 0$ as $T_c \rightarrow 0$ while $[S_\delta + S_u]/S_n \approx 1$ (within $\pm 10\%$) for all samples. Although some small amount of spectral weight may be transferred to high frequencies upon entering the superconducting state [14], our analysis shows that the vast majority remains at low frequencies.

Having located the “missing” spectral weight, we can consider a few possible reasons these charge carriers don’t condense. Perhaps the most obvious possibility is

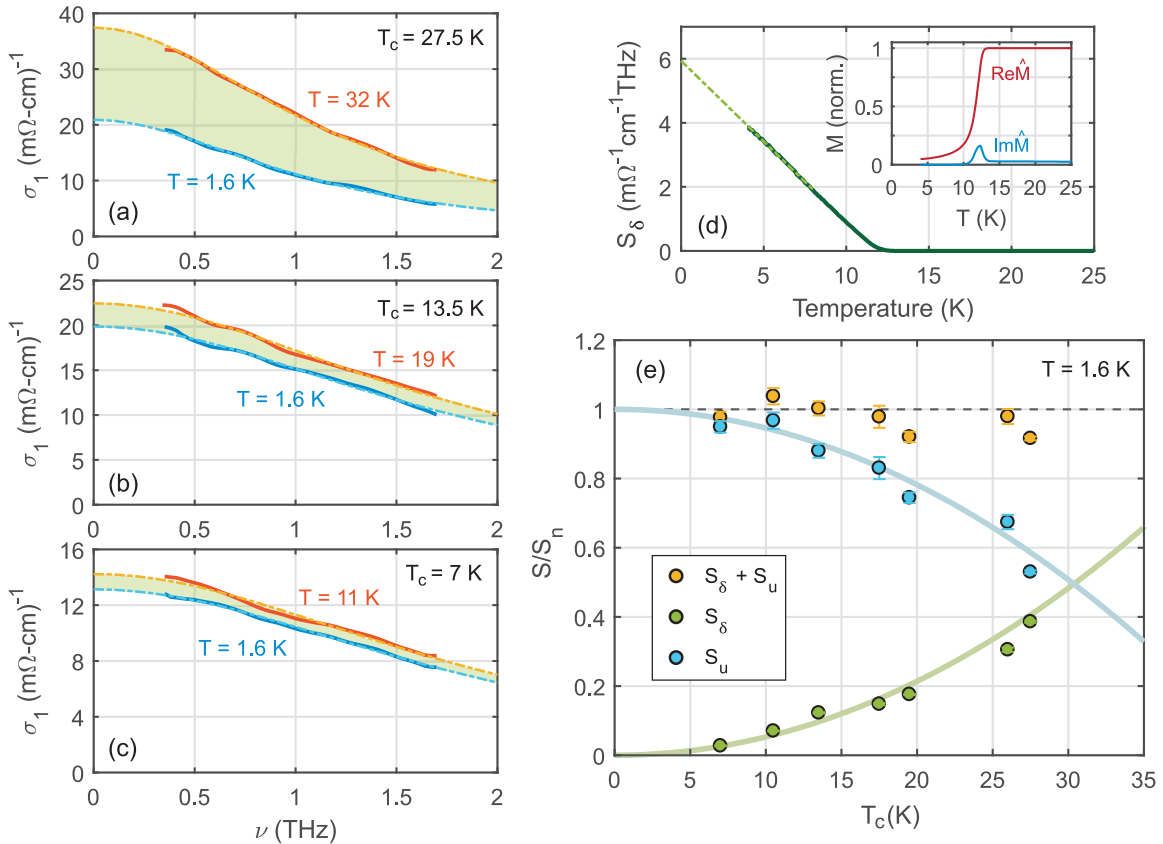


FIG. 2: **Sum rule analysis of the low frequency spectral weight** Comparison of the real part of the optical conductivity above and below T_c for overdoped $\text{La}_{2-x}\text{Sr}_x\text{CuO}_4$ films with (a) $T_c = 27.5$ K, (b) $T_c = 13.5$ K and (c) $T_c = 7$ K. Solid lines indicate the TDS data. Dashed lines show a Drude fit with a single scattering rate i.e. $\sigma_1(\nu) = S\tau/(1 + \nu^2\tau^2)$. Shaded green region represents the expected superfluid spectral weight. (d) The superfluid spectral weight S_δ with temperature for the film with $T_c = 13.5$ K as derived from the complex impedance using a two-coil setup ($\nu = 40$ kHz). The dashed line represents a linear extrapolation to determine S_δ for $T = 1.6$ K. Inset: The real and imaginary parts of the mutual inductance with temperature for the same film. (e) Spectral weight, normalized to the normal state spectral weight S_n , for the superfluid (S_δ) and for uncondensed spectral weight (S_u) as a function of doping at $T = 1.6$ K. S_δ is determined from the mutual inductance data as in (d) while S_u and S_n are determined from Drude fits to $\sigma_1(\nu)$. Yellow circles give $(S_\delta + S_u)/S_n$. Solid lines are guides to the eye. Error bars represent the 95% confidence interval (2 s.d.) in the fitting procedure to extract S .

pair-breaking scattering due to impurities which smears out the d -wave node leading to nodal Bogoliubov quasiparticles and a suppression of the superfluid density n_s . Pair-breaking as such in both the unitary and Born scattering limits have been studied extensively [15–19]. It was also recently considered by Lee-Hone et. al. [20] to explain the suppression in superfluid density observed in [1] by relying on mostly weak (Born) impurity scattering within a weak-coupling BCS theory. Our optical conductivity results presented here seem to be inconsistent with these models as previously implemented for the following reasons.

First, aside from the delta function at $\nu = 0$, $\sigma_1(\nu)$ for a dirty d -wave superconductor may be composed of both a narrow low frequency Drude-like peak and – if the normal state scattering rate is larger than the superconducting gap $2\Delta/h$ – a part that is an increasing function of ν (e.g. [21, 22]). For weak-coupling d -wave BCS, $2\Delta = 4.28k_B T_c$ and thus, $2\Delta/h$ is expected to

range from 0.62 THz to 2.45 THz for the films studied here i.e. comparable to the spectral range of our spectrometer. Yet, we do not observe any signatures of 2Δ compatible with this theory in our measured $\sigma_1(\nu)$ at the lowest temperature (Fig. 2a-c and SI Fig. S5). This means that the superconducting gap may be larger than expected from weak-coupling BCS and remains reasonably large as the critical doping is approached, or the gap’s signature is otherwise suppressed in the spectra. Additionally, while the zero-frequency limit of the residual $\sigma_1(\nu)$ can be sizable within dirty d -wave theory [18], the corresponding frequency dependence of the low frequency conductivity peak is not expected within existing theory (except in the unitary limit) to be the simple form of the single Lorentzian that we observe.

Second, it is expected that impurity scattering drives a change from the expected linear- T behavior of n_s for a clean d -wave superconductor to a quadratic dependence at a crossover temperature T^{**} for both strong (unitary)

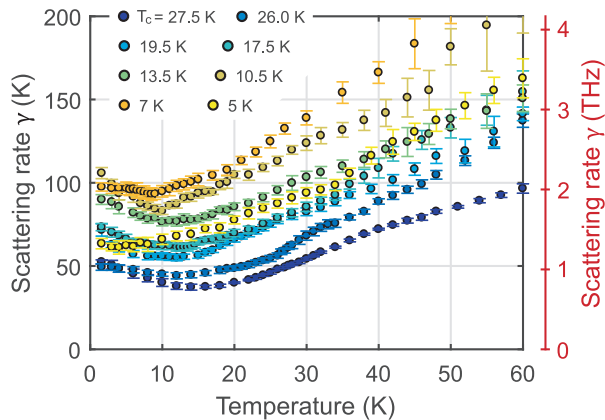


FIG. 3: **Scattering rate $\gamma > T_c$ for all films.** γ , in units Kelvin, with temperature for all films measured. γ is obtained with a single Drude-fit to $\sigma_1(\nu)$ at all temperatures as shown in Fig.2 a-c. Error bars represent the 95% confidence interval in the fitting procedure to extract the parameter $\gamma = 1/\tau$.

and weak (Born) scatterers [15–17, 19]. Irrespective of the kind of scattering, within extant theory T^{**} reflects a frequency scale γ that is roughly the width of the residual Drude peak $1/\tau$ in the limit $T \rightarrow 0$ as $T^{**} \simeq \gamma = 1/\tau$ [16]. Figure 3 shows the extracted scattering rate $\gamma = 1/\tau$ with temperature for all the films studied in this work. For each film, $\gamma \gtrsim T_c$ and thus T^{**} should be $\gtrsim T_c$. This implies that n_s should scale quadratically with T for all $T < T_c$. On the contrary, in all the present films as well as in the previous work [1], n_s remains quite linear down to the lowest temperatures (Fig. 2d) and no crossover behavior is observed. This demonstrates that our observed zero frequency peak is unlikely to be explained by existing theories of impurity scattering in a BCS type d -wave superconductor.

Observations reminiscent to ours have been made in heat capacity measurements of overdoped $\text{La}_{2-x}\text{Sr}_x\text{CuO}_4$ single crystals [23], where a large fermion-like linear-in- T contribution to the heat capacity was found deep into the superconducting state. For overdoped samples with $T_c \sim 20$ K the heat capacity coefficient was roughly 70% of the normal state and reached essentially 100% by $T_c \sim 7$ K. The most straightforward interpretation of such data is microscopic electronic phase separation i.e. the presence of superconducting regions embedded in a normal state metallic background. Our measurements support such a scenario in that the scattering rate of our low temperature residual Drude is about the same as that in the normal state (Fig. 3). However if our residual Drude peak were due to such phase separation then the volume fraction corresponding to the normal metallic region needs to be exceedingly large (e.g. nearly 95% for the film with $T_c = 7$ K). It is hard to reconcile robust bulk superconductivity as well as the exceedingly uniform T_c for all the films measured (as characterized by a sharp transition ($\Delta T_c < 0.5$ K) in the dissipative part of the mutual inductance

(Fig. 2d and [1])) with a scenario of such extreme phase separation.

A quantity that has been quite useful in understanding THz conductivity in previous works on the cuprates is the phase stiffness \mathcal{T}_ϕ , which is the energy scale to introduce twists in the phase ϕ of the superconducting order parameter $\Delta e^{i\phi}$. As detailed in previous works [11, 24, 25], in situations dominated by phase fluctuations, this quantity can be obtained from the imaginary part of the conductivity as $k_B \mathcal{T}_\phi = (h\nu\sigma_2 t)/G_Q$. \mathcal{T}_ϕ is then the two-dimensional stiffness of a single CuO_2 plane in units of degrees Kelvin, $G_Q = e^2/\hbar$ is the quantum of conductance and t is CuO_2 plane spacing. Measuring \mathcal{T}_ϕ at a finite frequency sets a length/time scale over which the system is dynamically probed. In the absence of fluctuations, the system will be stiff on all length and time scales and thus \mathcal{T}_ϕ should be independent of the probing frequency. In general, $\lim_{\nu \rightarrow \infty} \nu\sigma_2 = S_n$ i.e. the total spectral weight. Interpreting the residual Drude peak as uncondensed superconducting charge carriers allows us to study \mathcal{T}_ϕ as a function of frequency. We note that such an interpretation is similar to the analysis performed in Ref. [12] in which a residual conductivity peak in $\text{Bi}_2\text{Sr}_2\text{CaCu}_2\text{O}_{8+\delta}$ was interpreted as arising from a superconducting collective mode. However, even in the absence of such an interpretation, analyzing $\nu\sigma_2$ allows us to get a good picture of the distribution of the low frequency spectral weight.

Figure 4a shows $\nu\sigma_2$ (normalized to the normal state spectral weight S_n) at $T = 1.6$ K as a function of frequency between 0.3 and 1.7 THz for all films measured by TDTS. Note that the σ_2 considered here has been corrected from its measured value to take into account a small contribution from dielectric screening (see SI). We also plot in Fig. 4a the relative superfluid spectral weight (S_δ/S_n) as obtained from MI measurements at $\nu = 40$ kHz on the same films to directly compare in the low frequency limit. For all dopings, $\nu\sigma_2$ as measured in the high frequency region can be smoothly connected with the low frequency MI measurement. As can be seen, this quantity is strongly increasing with probing frequency for all dopings. In systems where the entire σ_2 arises from superconducting correlations, such dependence indicates that the phase of the system appears “stiffer” when probed at higher frequencies (i.e. at shorter length and time scales) but fluctuations degrade the superconductivity on longer length and time scales. This perspective has been used previously to analyze the THz response of the thermally fluctuating regime above T_c [11, 24, 25]. Additionally, we observe that $\nu\sigma_2 \rightarrow S_n$ as $\nu \rightarrow \infty$, in accordance with Kramer-Kronig relations for optical conductivity (also shown in SI sec. D). This independently validates our earlier analysis of $\sigma(\nu)$ in terms of a single Drude-like peak.

Note that one expects large phase fluctuations to accompany the decrease of the zero frequency superfluid phase stiffness. The fact that we measure the inductive response of the system over almost eight orders of

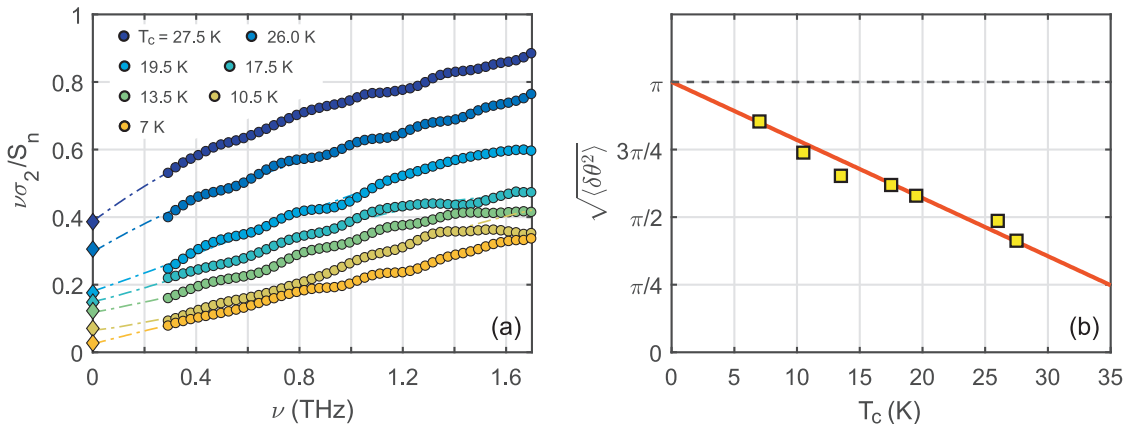


FIG. 4: **Superfluid phase stiffness at different length/time scales.** (a) $\nu\sigma_2$, normalized to the normal state spectral weight, versus frequency for all films at $T = 1.6$ K. $\nu\sigma_2$ is proportional to the superfluid phase stiffness \mathcal{T}_ϕ . Circle and diamond symbols represent the TDS and MI data respectively. Dashed lines are guides to the eye. (b) The average phase uncertainty determined from the quantum Debye Waller factor $W_Q = e^{-\langle\delta\theta^2\rangle/2}$ as a function of doping. W_Q is defined as the ratio of low and high frequency limits of \mathcal{T}_ϕ which is given by the suppression of the superfluid density from its bare value i.e. $W_Q = S_\delta/S_n$. Red line is a linear guide to the eye to the data shown as yellow squares.

magnitude allows us to perform a unique analysis in this regard. Renormalization of the system's diamagnetic response can be described in terms of a quantum Debye-Waller factor W_Q [26–28] which has been used in theoretical works to parametrize this suppression of the renormalized superfluid density e.g. $W_Q = S_\delta/S_n$. In the context of the self-consistent harmonic approximation, W_Q can be directly related to the root mean phase uncertainty of the order parameter as $W_Q = e^{-\langle\delta\theta^2\rangle/2}$ [29, 30]. This approach has been invoked to describe global phase coherence in Josephson-junction arrays [29] and phase disordered s -wave superconductors [31]. This is an intermediate regime form that obviously cannot be valid in the critical regime itself. For the purpose of this analysis, we assume that the normal state quasiparticle conductivity just above T_c gives the spectral weight of the normal state diamagnetic response (S_n). Figure 4b shows the root mean phase uncertainty $\sqrt{\langle\delta\theta^2\rangle}$ determined from W_Q as a function of doping. Remarkably, as the critical doping is approached ($T_c \rightarrow 0$), the average phase disorder $\sqrt{\langle\delta\theta^2\rangle}$ extrapolates to π . The maximum T_c for the $\text{La}_{2-x}\text{Sr}_x\text{CuO}_4$ cuprate family (~ 45 K) is near $\sqrt{\langle\delta\theta^2\rangle} \rightarrow 0$. Obviously π is a significant natural scale for a phase disordering transition and we propose that this is a key indicator of strong quantum phase fluctuations at the termination of the superconducting dome. We note that $T_c \propto \sqrt{S_\delta}$ is expected to emerge from quantum phase fluctuations within the (3+1)D-XY universality class with $z = 1$. Indeed, this is the scaling found in Ref. [1], but only very near the QCP, around $0.25 < x < 0.26$ (as well as in earlier work [9]). The same was found to be true for extreme UD YBCO, but only for $0.054 < x < 0.057$ [19]. Note that

all the data analyzed here are either extrapolated to $T = 0$ or taken in a regime where the spectra are temperature independent. Therefore, unlike previous work that concentrated on thermal superconducting fluctuations [11, 24, 25], here any fluctuations are quantum in nature and are associated with the zero-point motion of the condensate.

This analysis may be suggestive that the $T = 0$ superconducting to metal transition in overdoped $\text{La}_{2-x}\text{Sr}_x\text{CuO}_4$ near its QCP may be thought of as melting of a phase ordered state reminiscent of the melting of a solid. In the latter case, melting occurs when the root mean vibration amplitude exceeds a certain threshold expressed as a fraction of the spacing between nearest neighbors [32]. In our case, complete melting of the superconducting phase order occurs when the root mean phase uncertainty $\sqrt{\langle\delta\theta^2\rangle} \sim \pi$, setting a new criteria for the zero temperature superconducting transition. Note that this analysis may hold independent of the mechanism for suppression of the superfluid density. In this regard, the phase uncertainty can be seen as a consequence of the reduced superfluid density and not a cause. Of course, close to the critical point fluctuations themselves reduce the superfluid density. This may be regime where the critical scaling is observed. A scenario of phase fluctuations does not obviously explain features like the large linear-in-temperature heat capacity for overdoped samples [23], and it could be that the ultimate picture needs to combine aspects of both quantum fluctuations and phase separation where the transition proceeds through the phase disordering of weak superconducting links.

[1] Božović, I., He, X., Wu, J., and Bollinger, A. T. *Nature* **536**(7616), 309–311 (2016).

[2] Keimer, B., Kivelson, S. A., Norman, M. R., Uchida,

- S., and Zaanen, J. *Nature* **518**(7538), 179–186 (2015).
- [3] Emery, V. J. and Kivelson, S. A. *Nature* **374**(6521), 434–437 (1995).
- [4] Platé, M., Mottershead, J. D. F., Elfimov, I. S., Peets, D. C., Liang, R., Bonn, D. A., Hardy, W. N., Chiuzbadian, S., Falub, M., Shi, M., Patthey, L., and Damascelli, A. *Phys. Rev. Lett.* **95**, 077001 (2005).
- [5] Vignolle, B., Carrington, A., Cooper, R. A., French, M. M. J., Mackenzie, A. P., Jaudet, C., Vignolles, D., Proust, C., and Hussey, N. E. *Nature* **455**(7215), 952–955 (2008).
- [6] Uemura, Y. J., Keren, A., Le, L. P., Luke, G. M., Wu, W. D., Kubo, Y., Manako, T., Shimakawa, Y., Subramanian, M., Cobb, J. L., and Markert, J. T. *Nature* **364**(6438), 605–607 (1993).
- [7] Niedermayer, C., Bernhard, C., Binniger, U., Glöckler, H., Tallon, J. L., Ansaldo, E. J., and Budnick, J. I. *Phys. Rev. Lett.* **71**, 1764–1767 (1993).
- [8] Locquet, J.-P., Jaccard, Y., Cretton, A., Williams, E. J., Arrouy, F., Mächler, E., Schneider, T., Fischer, O., and Martinoli, P. *Phys. Rev. B* **54**, 7481–7488 (1996).
- [9] Lemberger, T. R., Hetel, I., Tsukada, A., Naito, M., and Randeria, M. *Phys. Rev. B* **83**, 140507 (2011).
- [10] Rourke, P. M. C., Mouzopoulou, I., Xu, X., Panagopoulos, C., Wang, Y., Vignolle, B., Proust, C., Kurganova, E. V., Zeitler, U., Tanabe, Y., Adachi, T., Koike, Y., and Hussey, N. E. *Nature Physics* **7**(6), 455–458 (2011).
- [11] Corson, J., Malozzi, R., Orenstein, J., Eckstein, J. N., and Božović, I. *Nature* **398**(6724), 221–223 (1999).
- [12] Corson, J., Orenstein, J., Oh, S., O’Donnell, J., and Eckstein, J. N. *Phys. Rev. Lett.* **85**, 2569–2572 (2000).
- [13] Corson, J., Orenstein, J., Eckstein, J., and Božović, I. *Physica B: Condensed Matter* **280**(1), 212–213 (2000).
- [14] Molegraaf, H., Presura, C., van der Marel, D., Kes, P., and Li, M. *Science* **295**(5563), 2239–2241 (2002).
- [15] Hirschfeld, P. J., Putikka, W. O., and Scalapino, D. J. *Phys. Rev. Lett.* **71**, 3705–3708 (1993).
- [16] Hirschfeld, P. J. and Goldenfeld, N. *Phys. Rev. B* **48**, 4219–4222 (1993).
- [17] Hosseini, A., Harris, R., Kamal, S., Dosanjh, P., Preston, J., Liang, R., Hardy, W. N., and Bonn, D. A. *Phys. Rev. B* **60**, 1349–1359 (1999).
- [18] Durst, A. C. and Lee, P. A. *Phys. Rev. B* **62**, 1270–1290 (2000).
- [19] Broun, D. M., Huttema, W. A., Turner, P. J., Özcan, S., Morgan, B., Liang, R., Hardy, W. N., and Bonn, D. A. *Phys. Rev. Lett.* **99**, 237003 (2007).
- [20] Lee-Hone, N. R., Dodge, J. S., and Broun, D. M. *Phys. Rev. B* **96**, 024501 (2017).
- [21] Won, H. and Maki, K. *Phys. Rev. B* **49**, 1397–1402 (1994).
- [22] Tajima, S., Fudamoto, Y., Kakeshita, T., Gorshunov, B., Železný, V., Kojima, K. M., Dressel, M., and Uchida, S. *Phys. Rev. B* **71**, 094508 (2005).
- [23] Wang, Y., Yan, J., Shan, L., Wen, H.-H., Tanabe, Y., Adachi, T., and Koike, Y. *Phys. Rev. B* **76**, 064512 (2007).
- [24] Bilbro, L. S., Aguilar, R. V., Logvenov, G., Pelleg, O., Božović, I., and Armitage, N. P. *Nature Physics* **7**(4), 298–302 (2011).
- [25] Bilbro, L. S., Valdés Aguilar, R., Logvenov, G., Bozovic, I., and Armitage, N. P. *Phys. Rev. B* **84**, 100511 (2011).
- [26] Ioffe, L. B. *Science* **285**(5431), 1241–1244 (1999).
- [27] Benfatto, L., Caprara, S., Castellani, C., Paramekanti, A., and Randeria, M. *Phys. Rev. B* **63**, 174513 (2001).
- [28] Kwon, H.-J., Dorsey, A. T., and Hirschfeld, P. J. *Phys. Rev. Lett.* **86**, 3875–3878 (2001).
- [29] Chakravarty, S., Ingold, G.-L., Kivelson, S., and Luther, A. *Phys. Rev. Lett.* **56**, 2303–2306 (1986).
- [30] Emery, V. J. and Kivelson, S. A. *Phys. Rev. Lett.* **74**, 3253–3256 (1995).
- [31] Mondal, M., Kamlapure, A., Chand, M., Saraswat, G., Kumar, S., Jesudasan, J., Benfatto, L., Tripathi, V., and Raychaudhuri, P. *Phys. Rev. Lett.* **106**, 047001 (2011).
- [32] Lindemann, F. *Physik. Z.* **11**, 609–612 (1910).
- [33] He, X., Gozar, A., Sundling, R., and Božović, I. *Review of Scientific Instruments* **87**(11), 113903 (2016).

METHODS

The complex conductivity was determined by time-domain THz spectroscopy. A femtosecond laser pulse is split along two paths and excites a pair of photoconductive ‘Austin’-switch antennae grown on LT-GaAs wafers. A broadband THz range pulse is emitted by one antenna, transmitted through the LSCO film, and measured at the other antenna. By varying the length-difference of the two paths, we map out the entire electric field of the transmitted pulse as a function of time. Comparing the Fourier transform of the transmission through LSCO to that of a reference resolves the full complex transmission. We then invert the transmission to obtain the complex conductivity via the standard formula for thin films on a substrate: $\hat{T}(\nu) = \frac{1+n}{1+n+Z_0\hat{\sigma}(\nu)d} e^{i\Phi_s}$ where Φ_s is the phase accumulated from the small difference in thickness between the sample and reference substrates and n is the substrate index of refraction. By measuring both the magnitude and phase of the transmission, this inversion to conductivity is done directly and does not require a Kramers-Kronig transformation.

The LSCO films were deposited on 1-mm-thick single-crystal LaSrAlO₄ substrates, epitaxially polished perpendicular to the (001) direction, by atomic-layer-by-layer molecular-beam-epitaxy (ALL-MBE). The samples were characterized by reflection high-energy electron diffraction, atomic force microscopy, X-ray diffraction, and resistivity and magnetization measurements, all of which indicate excellent film quality. All the films studied in this work are 20 monolayers thick (one monolayer is $\approx 6.6 \text{ \AA}$).

The superfluid spectral weight in the delta function S_δ is determined by a two-coil mutual inductance technique. For a superconducting film of thickness d and infinite radius placed between two coils of radii R_1 and R_2 parallel to one another and separated by a distance D , the complex mutual inductance can be written as:

$$\begin{aligned} \hat{M} &= \text{Re}M + i\text{Im}M \\ &= \mu_0\pi R_1 R_2 \frac{\int_0^\infty dq [\exp(-\mathbf{q}D) J_1(\mathbf{q}R_1) J_1(\mathbf{q}R_2)]}{\cosh(Qd) + [(Q^2 + \mathbf{q}^2)/2\mathbf{q}Q] \sinh(Qd)} \end{aligned}$$

where \mathbf{q} is the wave-vector, $J_1(x)$ is the first order Bessel function, $Q^2 = q^2 + (1/\lambda^2) - i\mu_0\omega\sigma_1$ and $\sigma_2 = 1/\mu_0\omega\lambda^2$. This can be generalized to the case of two solenoids with N_1 and N_2 turns respectively by the summation over each pair of coils. $\text{Re}M$ and $\text{Im}M$ are measured experimentally and the above equation is numerically inverted using the

algorithm outlined in [33] to obtain λ and σ_1 from which the superfluid spectral weight is calculated as $S_\delta = \frac{1}{2\pi\mu_0\lambda^2}$. Further details on the mutual inductance setup can be obtained in the Methods section of [1].

ADDITIONAL INFORMATION

Acknowledgments: The authors would like to thank L. Benfatto, D. Broun, D. Chaudhuri, D. Chowdhury, S. Dodge, P. Hirschfeld, S. Kivelson, M. Mondal, C. Varma, and I. Vishik, for helpful discussions. Research at JHU was funded by the US DOE, Office of Basic Energy Sciences, Division of Materials Sciences and Engineering through Grant No. DE-FG02-08ER46544. Film synthesis by molecular beam epitaxy and characterization was done at BNL and was supported by the U.S. Department of

Energy, Basic Energy Sciences, Materials Sciences and Engineering Division. X.H. is supported by the Gordon and Betty Moore Foundation's EPiQS Initiative through Grant GBMF4410 to I.B.

Author Contributions: F.M. performed the TDTS measurements, analyzed the data and wrote the initial draft of the text. X.H. and I.B. synthesized the films using ALL-MBE and carried out the mutual inductance measurements. N.P.A. conceived and supervised the project. All authors contributed to the understanding of the data and writing of the manuscript.

Competing Interests: The authors declare that they have no competing financial interests.

Correspondence: Correspondence and requests for materials should be addressed to F.M. (fahad@jhu.edu) or N.P.A. (npa@pha.jhu.edu).

Supplementary information

Locating the missing superconducting electrons in overdoped cuprates

Fahad Mahmood,¹ Xi He,^{2,3} Ivan Božović,^{2,3} and N. P. Armitage¹

¹*The Institute for Quantum Matter, Department of Physics and Astronomy,
The Johns Hopkins University, Baltimore, MD 21218 USA.*

²*Brookhaven National Laboratory, Upton, NY 11973, USA.*

³*Applied Physics Department, Yale University, New Haven, Connecticut 06520, USA.*

A. Measured complex conductivity for all films

Here we present the measured raw data, $\sigma_1(\nu)$ and $\sigma_2(\nu)$, for each film studied in this work at various temperatures (Fig. S1 to Fig. S6). The results for the film with the $T_c = 27.5$ K are shown in Fig. 1a,b of the main text. $\sigma_1(\nu)$ and $\sigma_2(\nu)$ are extracted from the measured complex transmission $\tilde{T}(\omega)$ as outlined in the Methods section of the main text i.e. :

$$\tilde{T}(\nu) = \frac{1+n}{1+n+Z_0\tilde{\sigma}(\nu)d} e^{i\Phi_s} \quad (1)$$

where Φ_s is the phase accumulated from the small difference in thickness between the sample and reference substrates and n is the substrate index of refraction. n is determined by an independent measure of the complex transmission of the reference substrate while Φ_s is determined by setting $\sigma_2(\nu) = 0$ in the complex transmission at room temperature ($T = 295$ K), which is the case for frequencies much less than the scattering rate.

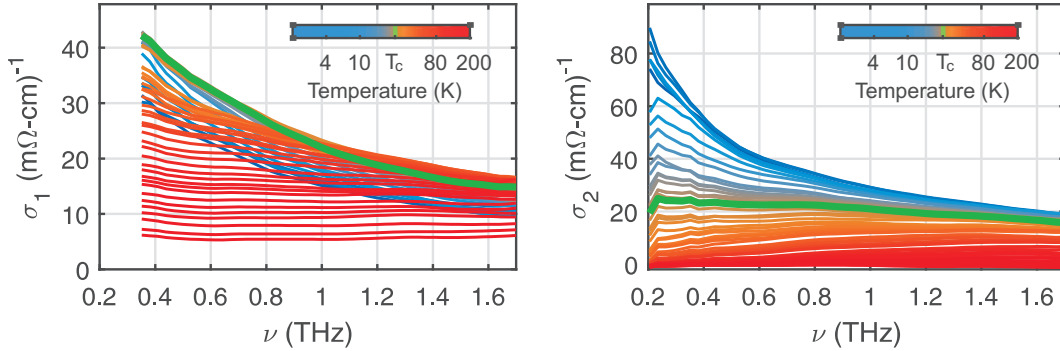


FIG. S1: THz optical conductivity of an overdoped $\text{La}_{2-x}\text{Sr}_x\text{CuO}_4$ thin film at various temperatures with $T_c = 26$ K

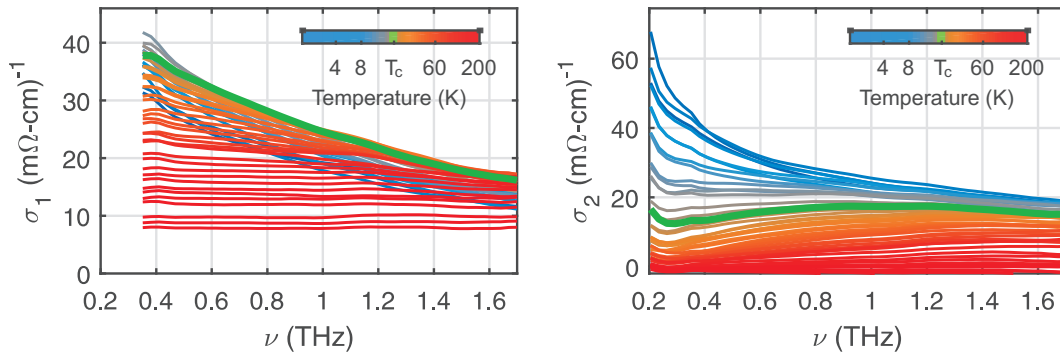
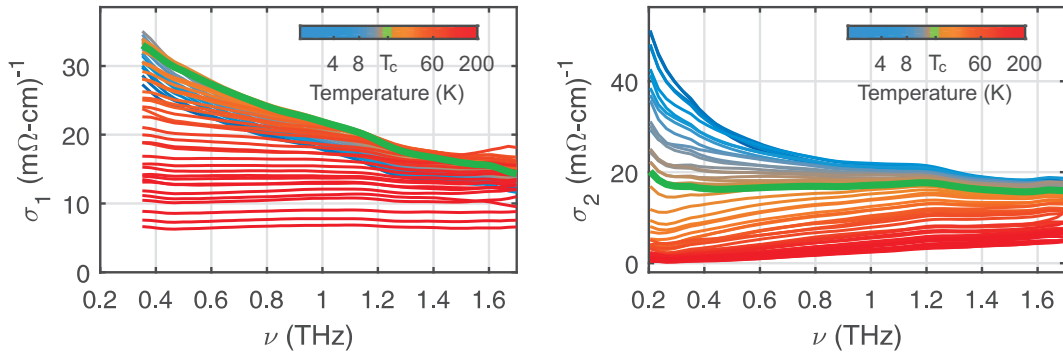
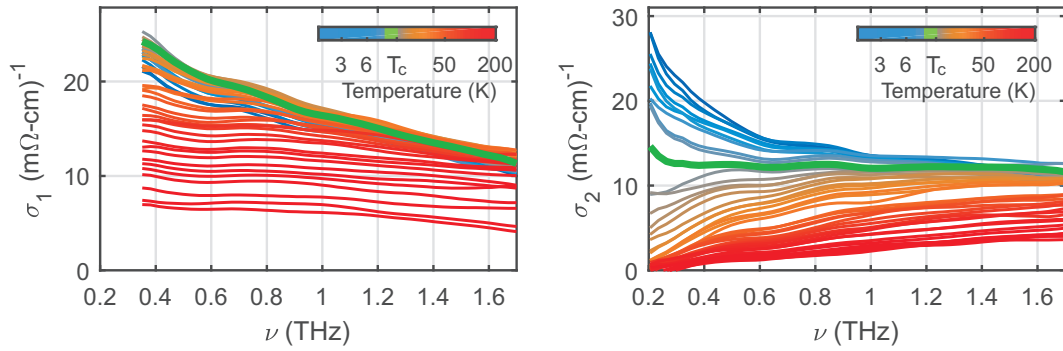
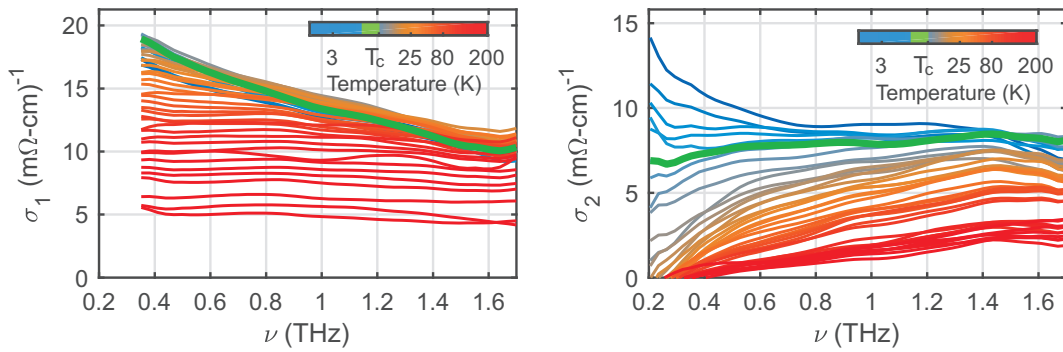
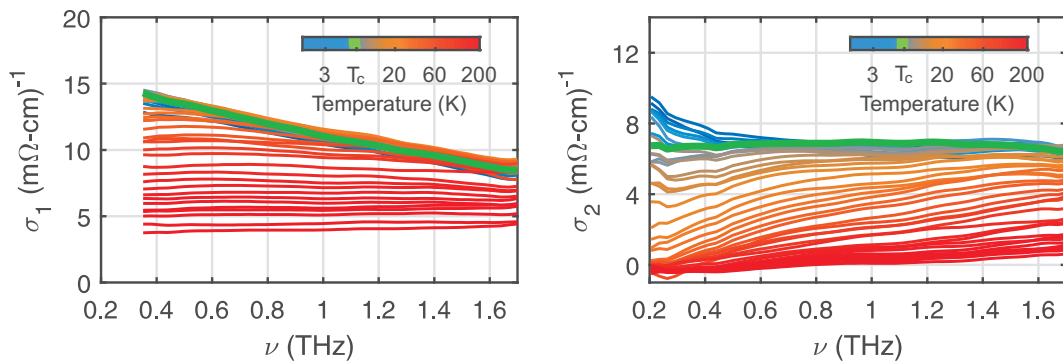


FIG. S2: THz optical conductivity of film with $T_c = 19.5$ K

FIG. S3: THz optical conductivity of film with $T_c = 17.5$ KFIG. S4: THz optical conductivity of film with $T_c = 13.5$ KFIG. S5: THz optical conductivity of film with $T_c = 10.5$ KFIG. S6: THz optical conductivity of film with $T_c = 7$ K

B. Fits to extract S_u and S_n from $\sigma_1(\nu)$

As discussed in the main text, $\sigma_1(\nu)$ for each film can be fit to a single Drude to extract the uncondensed (S_u) and normal state (S_n) spectral weight along with the scattering rate (τ). The fits for films with $T_c = 27.5$ K, 13.5 K and 7 K are shown in Fig. 2a, 2b and 2c of the main text, respectively. The fits for the other four films are shown here in Fig. S7.

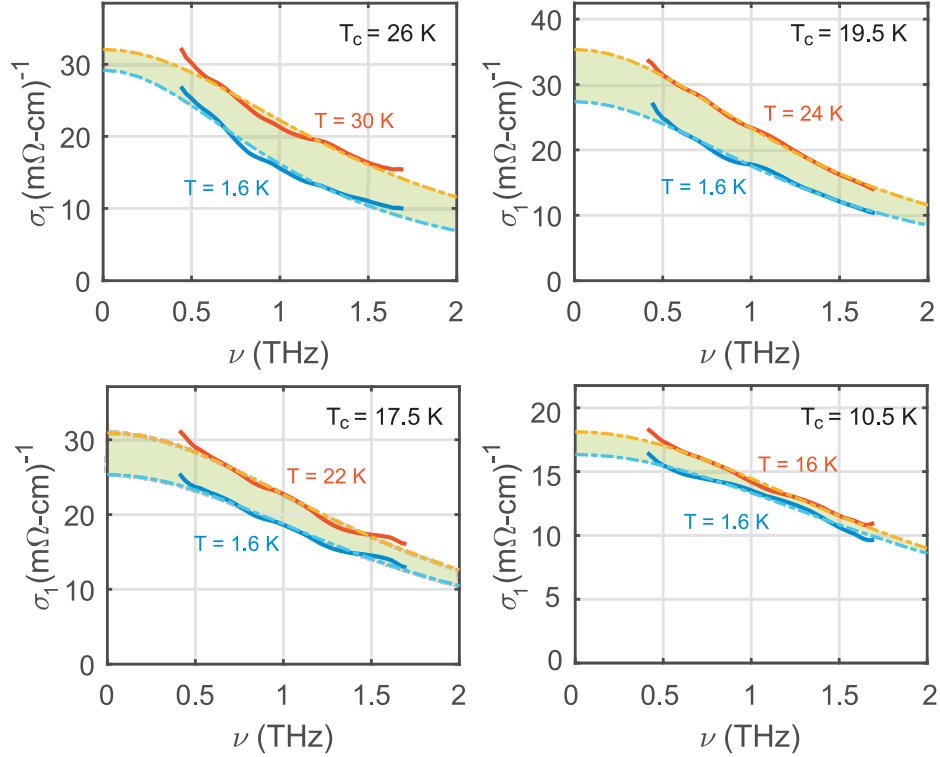


FIG. S7: Fits to extract S_u and S_n from $\sigma_1(\nu)$. Comparison of the real part of the optical conductivity above and below T_c for three of the $\text{La}_{2-x}\text{Sr}_x\text{CuO}_4$ films. Data for the other three films are presented in the main text. Solid lines indicate the TDTs data. Dashed lines show a Drude fit with a single scattering rate i.e. $\sigma_1(\nu) = S\tau/(1 + \nu^2\tau^2)$. Shaded green region represents the expected superfluid spectral weight.

C. Contribution to $\sigma_2(\nu)$ from high frequency absorption

In this section we study whether absorption at frequencies much greater than the setup's spectral range contributes to the measured imaginary part of the complex conductivity i.e. $\sigma_{2,m}(\nu)$. Such excitations will give a contribution to the low frequency dielectric constant that should be removed from $\sigma_{2,m}(\nu)$ before converting it to a phase stiffness. Due to the Kramers-Kronig relation for optical conductivity as stated below, a finite $\sigma_{1,m}(\nu)$ at high frequencies (absorption) can lead to a measurable $\sigma_{2,m}(\nu)$ at low frequencies:

$$\sigma_{2,m}(\nu) = -\frac{2\nu}{\pi} \mathcal{P} \int_0^\infty \frac{\sigma_{1,m}(\nu')}{\nu'^2 - \nu^2} d\nu' \quad (2)$$

To consider if that is the case in our measurements, we study the metallic normal state conductivity of the films ~ 50 K above T_c . As noted in the main text, the normal state $\sigma_{1,m}(\nu)$ at low frequencies is Drude-like and so the low frequency complex conductivity can be written as:

$$\sigma(\nu) = \frac{S\tau}{1 - i\nu\tau} + iE(\nu) = \sigma_{1,d}(\nu) + i\sigma_{2,d}(\nu) + iE(\nu) \quad (3)$$

where $\sigma_{1,d}(\nu) = S\tau/(1 + \nu^2\tau^2)$, $\sigma_{2,d}(\nu) = S\nu\tau^2/(1 + \nu^2\tau^2)$, and $E(\nu)$ is a real negative function. In Fig. S8, we plot $\sigma_{1,m}(\nu)$ and $\sigma_{2,m}(\nu)$ for each film measured at ~ 50 K above T_c . $\sigma_{1,m}(\nu)$ for each film can be fit to $\sigma_{1,d}(\nu)$

to extract the parameters S and τ from which $\sigma_{2,d}(\nu)$ is calculated. As can be seen, the measured imaginary conductivity $\sigma_{2,m}(\nu)$ does not match the calculated imaginary conductivity $\sigma_{2,d}(\nu)$, i.e., $\sigma_{2,m}(\nu) \neq \sigma_{2,d}(\nu)$, for films with $T_c = 27.5$ K and $T_c = 26$ K indicating that $E(\nu) \neq 0$ for these films. We find that for the metallic normal state $E(\nu) = \sigma_{2,m}(\nu) - \sigma_{2,d}(\nu)$ is independent of temperature within experimental uncertainty. Based on this, we make the reasonable assumption that the contribution of high-frequency absorption to $\sigma_{2,m}(\nu)$ below T_c is given by the function $E(\nu)$ as determined at ~ 50 K above T_c e.g. the temperature dependent changes to $E(\nu)$ are small. Based on this, $\nu\sigma_2$ plotted in Fig. 4a for $T = 1.6$ K in the main text is determined using $\sigma_2 = \sigma_{2,m} - E(\nu)$ to subtract out the high-frequency absorption contribution. Note that for films with $T_c = 19.5$ K, 17.5 K, 13.5 K, 10.5 K, and 7 K, $E(\nu) \approx 0$. Unnormalized $\nu\sigma_2$ (corrected with the $E(\nu)$ function) is plotted in Fig. S9.

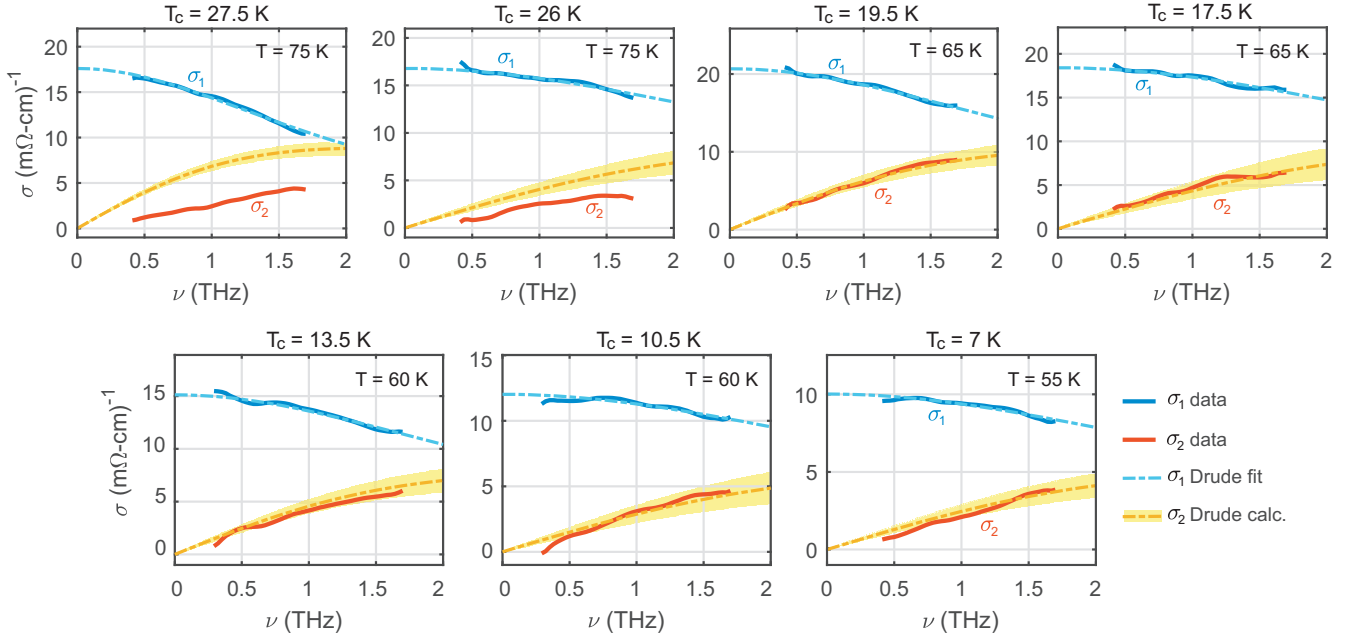


FIG. S8: Determining $E(\nu)$, the contribution to $\sigma_2(\nu)$ from high frequency absorption. For each film the measured $\sigma_{1,m}(\nu)$ at ~ 50 K above T_c is fit to a single Drude peak $S\tau/(1 + \nu^2\tau^2)$ (blue dashed line). The resulting $\sigma_{2,d}(\nu) = S\nu\tau^2/(1 + \nu^2\tau^2)$ is calculated and plotted as the orange dashed line with the shaded yellow region representing the 95% confidence interval in determining $\sigma_{2,d}(\nu)$ from the fitting parameters. $E(\nu)$ is given by $\sigma_{2,m}(\nu) - \sigma_{2,d}(\nu)$ for the films with $T_c = 27.5$ K and $T_c = 26$ K.

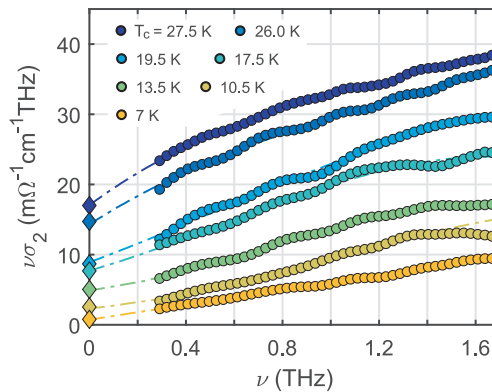


FIG. S9: $\nu\sigma_2$ versus frequency for all films at $T = 1.6$ K. $\nu\sigma_2$ is proportional to the superfluid phase stiffness \mathcal{T}_ϕ . Circle and diamond symbols represent the TDTs and two-coil mutual inductance data respectively. Dashed lines are guides to the eye.

D. Kramers-Kronig compatible analysis of $\sigma_1(\nu)$ and $\sigma_2(\nu)$

In our TDTS experiments, $\sigma_1(\nu)$ and $\sigma_2(\nu)$ are measured independently of each other. $\sigma_1(\nu)$ is then fit to a single Drude to extract the spectral weight and the scattering rate. To increase confidence in these fits, we show here that the measured $\sigma_2(\nu)$ is indeed compatible with the calculated $\sigma_2(\nu)$ from the Kramer-Kronig transform of the fitted $\sigma_1(\nu)$.

Figure S10 shows this comparison for the normal state data. For each film, the measured normal state $\sigma_1(\nu)$ is fit to a single Drude, i.e., $S\tau/(1 + \nu^2\tau^2)$ to obtain S and τ (also shown in Fig. 2 and Fig. S7). The resulting $\sigma_2(\nu)$ is then calculated as $S\nu\tau^2/(1 + \nu^2\tau^2)$ (Kramers-Kronig transform of the fitted $\sigma_1(\nu)$) and plotted as the orange dashed line to compare with the measured $\sigma_2(\nu)$ (red line). Note that the measured $\sigma_2(\nu)$ for the films with $T_c = 27.5$ K and $T_c = 26$ K is adjusted with the $E(\nu)$ function as discussed above in section C. As shown in Fig. S10, there is excellent agreement between the measured and calculated $\sigma_2(\nu)$.

For the superconducting state, the measured quantity of interest is $\nu\sigma_2$ as shown in Fig. 4a and Fig. S9. To see if this is consistent with the fitting to the residual $\sigma_1(\nu)$, we calculate $\nu\sigma_2$ as follows:

$$\nu\sigma_2 = S_\delta + \frac{S_u\nu^2\tau^2}{1 + \nu^2\tau^2} \quad (4)$$

where S_δ is the spectral weight in the superconducting state from MI measurements and the second term corresponds to the Kramers-Kronig transform of the fit to the measured $\sigma_1(\nu)$ at 1.6 K as shown in Fig. 2 and Fig. S7. We compare this calculated $\nu\sigma_2$ with the measured $\nu\sigma_2$ in Fig. S11. There is reasonably good agreement between the two for each film. Differences are likely due to small deviations from the exact Drude form for $\sigma_1(\nu)$. The systematic error for the film with $T_c = 27.5$ K is likely due to the error in the estimation of the $E(\nu)$ function.

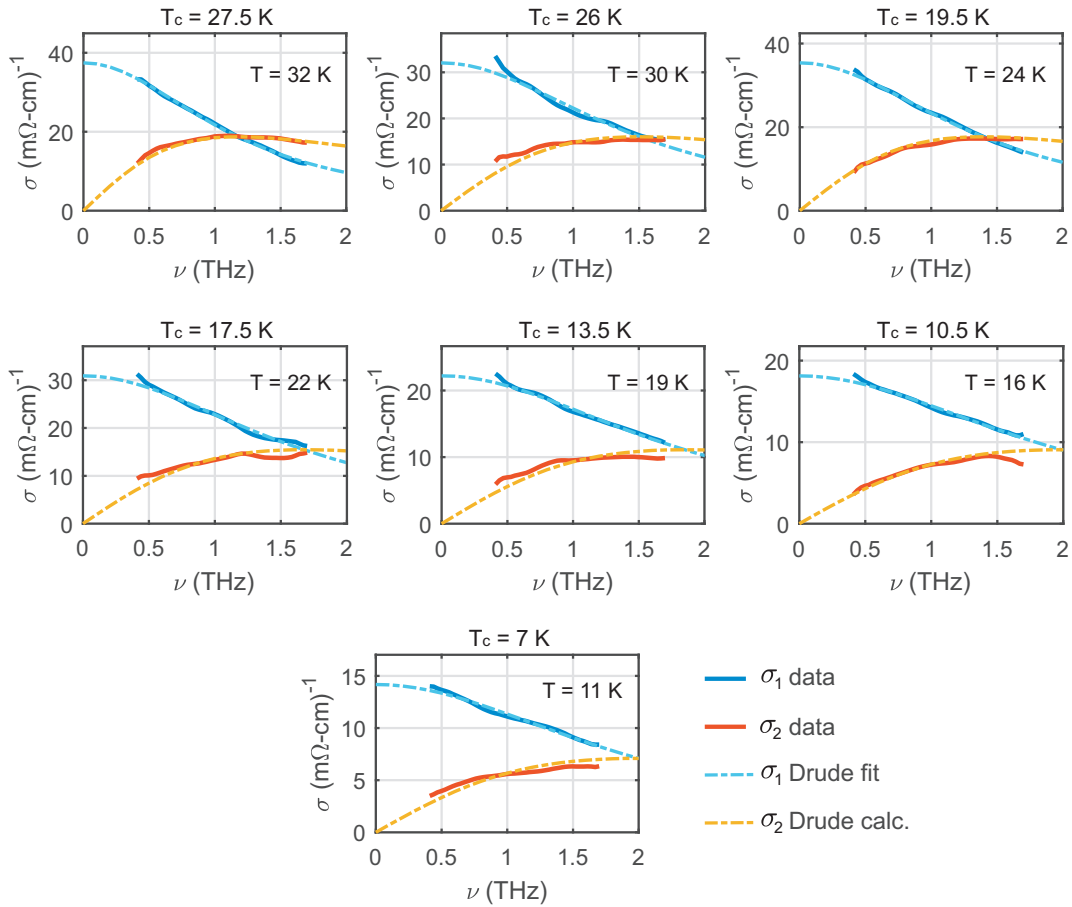


FIG. S10: Comparison of the measured and calculated normal state σ_2 for each film

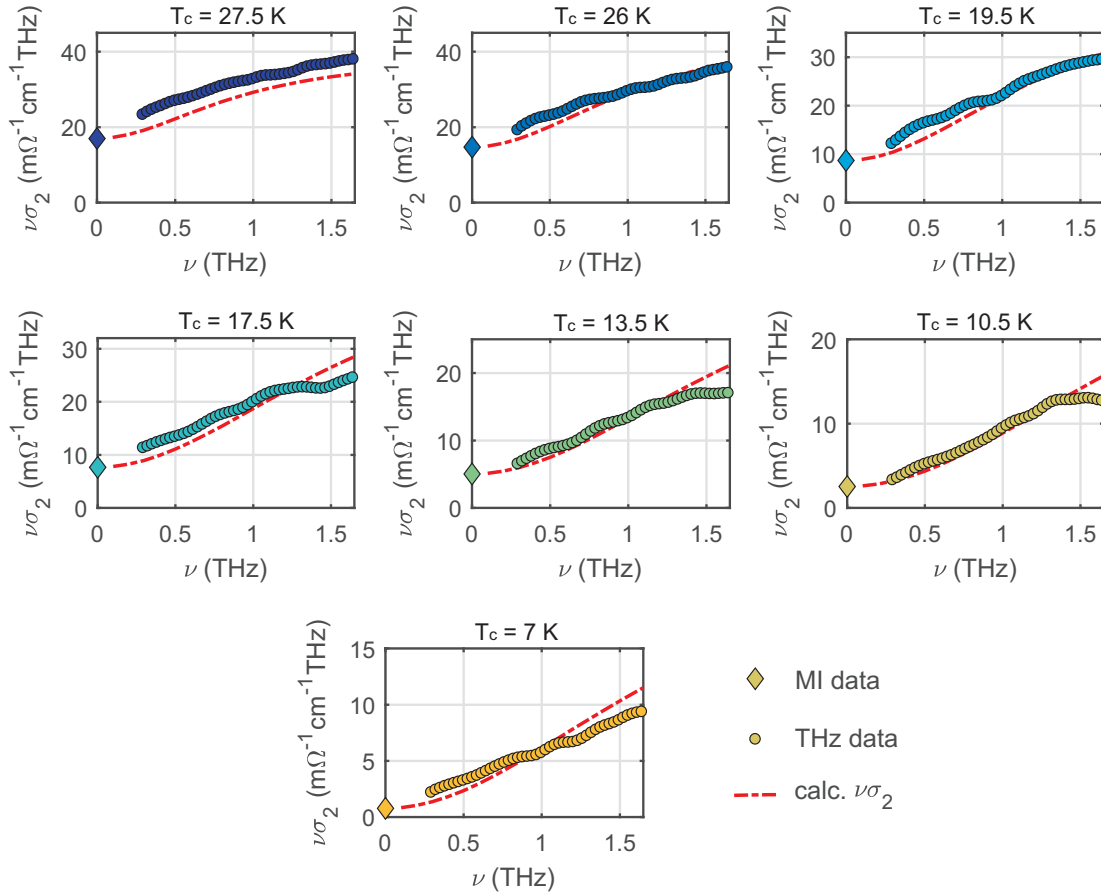


FIG. S11: Comparison of the measured and calculated $\nu\sigma_2$ at $T = 1.6$ K for each film

E. Spectral weights in absolute units

Figure 2e of the main text shows the residual (S_u) and superfluid (S_δ) spectral weights, normalized to the normal state (S_n) spectral weight, as a function of T_c . Here we plot the absolute spectral weights S_n , S_u and S_δ for each film (Fig. S12). In addition, we also plot the superfluid spectral weights for the films studied by Božović et.al. [Ref. 1] as $S_{\delta,(\text{ref.1})}$. This curve corresponds to the “ideal” relationship between the superfluid density and T_c for overdoped $\text{La}_{2-x}\text{Sr}_x\text{CuO}_4$ films. As can be seen, all the films presented in this work lie on this “ideal” curve.

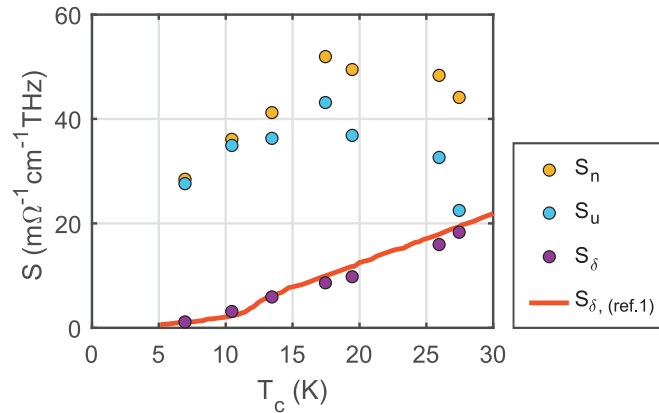


FIG. S12: Spectral weights in absolute units as a function of T_c . The red line is obtained from Božović et.al. [Ref. 1]

F. Comparison of d.c. transport and TDTS results

In this section, we compare the normal state $\nu \rightarrow 0$ real conductivity, $\sigma_1(0)$, as obtained from d.c. transport on small (300 μm by 100 μm) devices and from our TDTS experiments on large (1 cm by 1 cm) films (Fig. S13). The d.c. transport results are obtained from Božović et.al. [Ref. 1] at roughly 5 K above T_c for each doping. The TDTS results are from extrapolating the measured normal state $\sigma_1(\nu)$ to $\nu \rightarrow 0$ using Drude fits as shown in Fig. 2 and Fig. S7.

As shown in Fig. S13, the two techniques give roughly the same $\sigma_1(0)$ for lower dopings (higher T_c) but separate at higher dopings with $\sigma_1(0)$ measured on small devices using d.c. transport being greater than our TDTS results. We note here that all the films presented in Fig. S13 lie on the “ideal” superfluid density vs. T_c curve in Fig. S12. That is, the superfluid density and T_c does not seem to depend on the normal state $\sigma_1(0)$.

The discrepancy between the two methods is explained by oxygen vacancies. Overdoped $\text{La}_{2-x}\text{Sr}_x\text{CuO}_4$ for higher Sr concentrations is prone to the formation of oxygen vacancies. These vacancies can reduce the d.c. conductivity presumably due to an increase in scattering rate without affecting T_c in any significant way. Ozone annealing can be used to shift the conductivity up as it back-fills some oxygen and was carried out for the films shown Božović et.al. [Ref. 1]. However, ozone annealing only works well with small devices in d.c. transport experiments as oxygen diffusion is mostly lateral. Therefore, the conductivity of the film devices in Ref. 1 can be considered as the best case scenario and they will naturally have a higher d.c. conductivity than the un-patterned large films used for TDTS measurements.

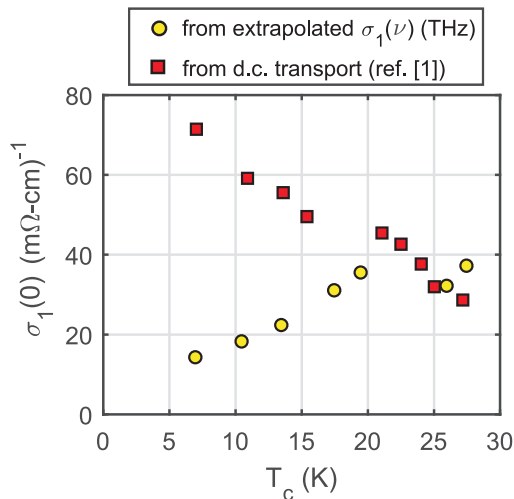


FIG. S13: Comparison of the normal state d.c. conductivity as obtained from transport experiments on small (micron) size devices and from extrapolating the measured TDTS $\sigma_1(\nu)$ for $\nu \rightarrow 0$. The d.c. transport results are obtained from Božović et.al. [Ref. 1]